AIAA JOURNAL
Vol. 44, No. 8, August 2006

Numerical Study of Evolution of Strongly Forced Axisymmetric Laminar Cold-Flow Jets

V. V. Barve,* O. A. Ezekoye,† and N. T. Clemens‡
University of Texas at Austin, Austin, Texas 78712
and
V. R. Katta§
Innovative Scientific Solutions, Inc., Dayton, Ohio 45440-3638

Periodic jet forcing presents interesting opportunities for jet mixing for a variety of applications. In this work, simulations are performed to study the effect of high-amplitude forcing on laminar jets ($Re = 100$) with net mass flux. For the cases presented in this work, we look at the effects of simulating the internal nozzle and show that assumptions about the nozzle flow have a large effect on the downstream flow evolution. Studies are performed on strongly forced axisymmetric jets in two geometries: 1) jets issuing perpendicularly from a flat wall and 2) jets issuing from a straight tube (nozzle). The amplitude and frequency of the forcing function are varied to study vortex creation and subsequent evolution downstream of the jet. For example, cases in which the peak jet velocity is three to four times the mean jet velocity are examined. The near-nozzle region was of particular interest due to the strong mixing processes occurring there. We discuss how nozzle flow processes modify the creation of downstream large-scale vortical structures. An interesting result of this work is that the strongest forcing cases possess some striking similarities to synthetic jets. For such cases, the flow reversal processes at the jet exit plane are investigated.

Nomenclature

A	=	amplitude of forcing
D	=	nozzle diameter
f	=	frequency of forcing
g	=	gravitational acceleration
Q	=	volumetric flow rate across cross section at distance x downstream of nozzle
Q_e	=	volumetric flow rate across nozzle exit
Re	=	Reynolds number, $U_0 D/\nu$
r	=	radial distance
Sr	=	Strouhal number, $f D/U_{\max}$
$U_{\max}$	=	maximum axial velocity (occurs at 25% phase)
U_0	=	time-averaged axial velocity
X	=	axial distance at which velocity oscillations are less 5% of time-averaged velocity
x	=	axial distance
ν	=	kinematic viscosity
ρ	=	density

I. Introduction

JET mixing is improved in laminar flows by unsteady forcing. The ability to increase the mixing rate for laminar flows is important in the development of mesoscale reactors of various types. In some small-scale (laminar) combustion reactors, acoustically excited and pulsed-flow flames have been shown to have significantly different characteristics in terms of flame length and luminosity when compared to nonpulsed flames. Forced jets have been studied in the literature for their ability to modify the flowfield and increase the jet entrainment rates. Significantly more work has been performed in the analysis of turbulent pulsed jets as compared to laminar jets because of the obvious technological applications of turbulent jets. However, with increased miniaturization of reactors of all types, the requirement for mixing in small-scale and laminar flows becomes more of an issue.[1,2] In addition, there may be similarities between turbulent and laminar unsteadily forced jets, and insights from one flow regime may aid in interpretation of observations in another regime. As such, we will review some of the more relevant turbulent unsteadily forced literature in this paper. The seminal work by Crow and Champagne[3] showed that jet forcing increased the entrainment rates for turbulent jets. They also found a preferred excitation mode at $Sr = 0.3$; note that their Strouhal number is based on the mean jet exit velocity and forcing frequency. Hill and Greene[4] and Vermuelen et al.[5] have also reported increased mixing rates and entrainment with periodically forced jets.

Marzouk et al.[6] performed simulations on weakly forced laminar jets. (The amplitude was less than 20% of the mean velocity.) The jet velocity profiles revealed that the effects of the forcing were restricted to the core of the jet. Also, they observed that the extent of the area affected by the forcing depended on the forcing frequency.

The forcing amplitudes used in all of the aforementioned cases did not fully modulate the flow, that is, the forcing amplitude was always less than 100%, and so there was no flow reversal at the nozzle exit. Increasing the forcing amplitude to the point where the flow is fully modulated allows for much more interesting flow dynamics. In reacting systems, such as that in the work of Shaddix et al.,[7] where a laminar reacting jet was periodically/acoustically forced, significant changes occurred in the flame characteristics. Later, particle image velocimetry (PIV) data for the same experimental conditions were acquired by Papadopoulos et al.,[8] and they showed that during certain phases, negative velocities are present in the near-nozzle region for moderately and strongly forced flames. This indicated that the fluid was being sucked back into the nozzle. Also, shadowgraphs indicated a strong mixing of the cool and hot regions due to the forcing. In other work, Muramatsu and Era[9] studied the mixing of pulsed CO_2 gas issuing from a round nozzle into still air. Velocity and concentration measurements revealed a phase lag between concentration and velocity, with the concentration changing after the velocity. Also, the mixing of gases was greatly enhanced near the nozzle exit and the mass fraction of the CO_2 at the nozzle exit

Received 1 June 2005; revision received 21 October 2005; accepted for publication 29 December 2005.

*Graduate Research Assistant, Department of Mechanical Engineering.
†Professor, Department of Mechanical Engineering; dezekoye@mail.utexas.edu.
‡Professor, Department of Aerospace Engineering. Associate Fellow AIAA.
§Senior Engineer, 2766 Indian Ripple Road. Associate Member AIAA.

was found to be lower than unity, indicating that air from the surroundings was being ingested into the nozzle during parts of the cycle.

It can be argued that synthetic jets, jets with zero net mass flux, can be considered to be a limiting case of strongly forced periodic jets, where the forcing amplitude is infinitely larger than the mean velocity. The flowfield developed by synthetic jets has been discussed in detail in the literature by Smith and Glezer,[10] Cater and Soria,[11] and Glezer and Amitay.[12] Cater and Soria[11] commented that synthetic jets are a special case of fully pulsed jets where the mean velocity of the jet is zero due to the pulsing action. They found that turbulent synthetic jets have similar cross-stream velocity profiles as steady jets, but with different spreading and decay rates. Direct numerical simulation studies by Rizzetta et al.[13] and Lee and Goldstein[14] of the synthetic jets used in the experiments of Smith and Glezer[10] provided further insight into the flowfield development of slot jets. Rizzetta et al.[13] presented two- and three-dimensional computational results. They simulated the oscillating membrane by applying a moving boundary condition and found that the flow in the cavity becomes periodic after several cycles. As a result, periodic velocity profiles could be used as the boundary condition at the slot exit to simulate the forcing action. The two-dimensional calculations by Lee and Goldstein[14] showed that the Reynolds number affected the slot exit flow profile, whereas the Strouhal number affected the jet evolution downstream of the slot. Bera et al.[15] used PIV to examine both pulsed jets, that is, strongly forced jets with net mass flux, and synthetic jets under identical forcing conditions and found that the synthetic jets have more lateral expansion than the pulsed jets.

In this study, two exit flow conditions are examined in terms of their influence on forced laminar jet evolution. We study forced laminar wall jets (issuing perpendicular to the wall) with top-hat exit velocity profiles and with fully developed velocity profiles. We also examine a jet flow issuing from a nozzle, that is, a straight tube five diameters in length, embedded in the computational domain. For both types of problems, the forcing frequency and the forcing amplitude are varied to examine their effects on jet evolution.

II. Numerical Scheme

A finite volume computational fluid dynamics (CFD) code, UNICORN, was used for the computations. This code solves the two-dimensional axisymmetric form of the unsteady conservation of momentum and conservation of mass equations using a staggered grid, where velocities take face values and where pressure and density are cell centered,

$$\frac{\partial \rho}{\partial t} + \nabla \cdot (\rho \boldsymbol{V}) = 0 \tag{1}$$

$$\rho \frac{\partial \boldsymbol{V}}{\partial t} + \rho \boldsymbol{V} \cdot \nabla \boldsymbol{V} = -\nabla P + \rho \boldsymbol{g} - \nabla \cdot \bar{\bar{\tau}} \tag{2}$$

The implicit form of the QUICKEST scheme is used for discretization of the momentum equation, and the pressure projection method is used to close the pressure/mass conservation relationship. The finite difference scheme is third-order accurate in space and third-order accurate in time. Katta et al.[16] provide further details about the numerical schemes and the individual terms in the descretized form of the continuity and momentum equations. The time-step size in the calculations is limited by the Courant–Friedrichs–Lewy condition, viz.,

$$u(\Delta t/\Delta x) \leq 1 \tag{3}$$

The iterative alternate direction implicit scheme is used to solve the momentum equations. The iterations are stopped once the values of the velocity components converge to a small value:

$$(\varphi^n - \varphi^{n-1})/\varphi^{n-1} \leq 10^{-5} \qquad \text{or} \qquad \varphi^n - \varphi^{n-1} \leq 10^{-5} \tag{4}$$

where φ is the velocity component.

The pressure Poisson equation is set up based on the continuity equation and is solved directly using the lower–upper decomposition method.

Two physical situations (domains) were modeled in this study. The first one, shown in Fig. 1a, involves a wall jet in which the computational domain is stretched to 12 cm in the radial direction and 40 cm in the axial direction. A nonuniform grid, with 410 points in the axial direction and 224 points in the radial direction, was used. The grid lines were clustered in the shear-layer region near the jet exit and varied in size from 0.01 to 0.4 cm axially and from 0.01 to 0.17 cm radially. Outflow (zero-gradient) boundary conditions are applied at the right side and top boundaries, whereas symmetry boundary conditions are applied along the centerline. The bottom side incorporates the wall jet; an inlet velocity boundary condition is specified over the radial extent of 0.5 cm, and the wall boundary condition covers the remainder of the boundary.

The second domain (Fig. 1b) is an extension of the first domain to explore the effects of a nozzle. Once again the diameter of the jet is kept at 1 cm, but the nozzle extends 5 cm into the domain. The

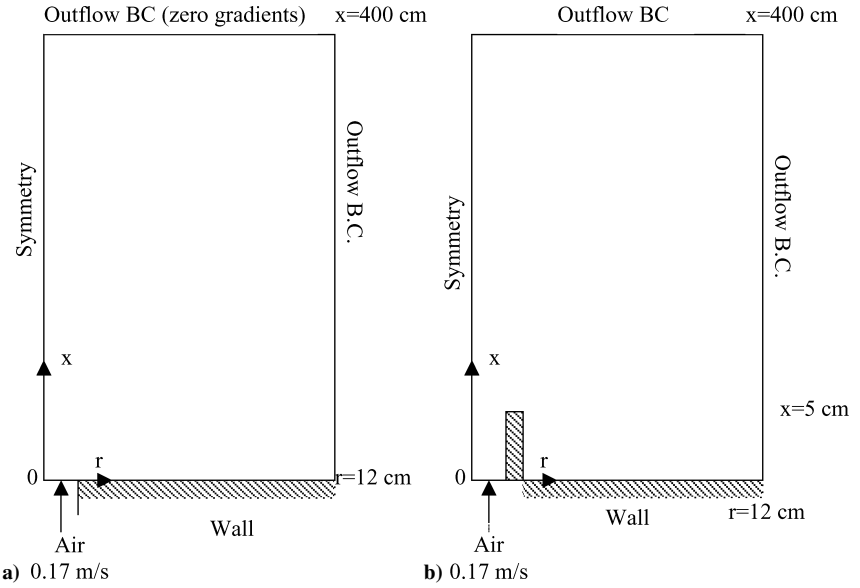

Fig. 1 Schematic of computational domain (not to scale): a) computational domain of wall jet and b) domain for nozzle jet.

Table 1 Different conditions (amplitude and frequency) and geometries examined

Geometry	U_0	$Re(U_0 D/\nu)$	A, %	f, Hz	Sr ($fD/U_{\max}$)
Wall jet	0.17	100	200	2.5	0.049
Wall jet	0.17	100	200	5	0.098
Wall jet	0.17	100	200	10	0.196
Wall jet	0.17	100	200	16	0.314
Wall jet	0.17	100	200	50	0.98
Wall jet	0.17	100	200	100	1.961
Wall jet	0.17	100	200	200	3.922
Wall jet	0.17	100	200	500	9.804
Wall jet	0.17	100	300	5	0.074
Wall jet	0.17	100	300	50	0.735
Wall jet	0.17	100	300	100	1.471
Wall jet	0.17	100	300	200	2.941
Wall jet	0.17	100	300	500	7.353
Wall jet	0.17	100	1000	50	0.267
Wall jet	0.51	300	200	50	0.327
Wall jet	0.51	300	200	500	3.268
Wall jet	0.51	300	300	500	2.451
Wall jet	0.34 (FD)[a]	100	200	5	0.049
Wall jet	0.34 (FD)	100	200	50	0.49
Wall jet	0.34 (FD)	100	200	500	4.902
Nozzle	0.17	100	200	5	0.098
Nozzle	0.17	100	200	50	0.98
Nozzle	0.17	100	200	500	9.804

[a]FD indicates fully developed velocity profile, with the peak velocity being listed. All other cases have top-hat velocity profile.

nozzle wall thickness was 0.1 cm. The domain extends 400 cm from the nozzle tip in the axial direction and 12 cm from the centerline in the radial direction. Once again, outflow boundary conditions are applied to the top and left side boundaries and a symmetry boundary condition was applied at the centerline. In this case, the jet velocity at the bottom of the nozzle was described.

A steady-state jet was simulated to benchmark the code and the numerical scheme. This involved an air jet issuing out into quiescent surroundings (air). This steady-state jet solution then served as the initial condition for the forced jets. For all of the simulations, properties of air at 300 K and 1 atm were used. The baseline case is a steady jet with a top-hat velocity profile of magnitude 17 cm/s. The diameter of the jet was 1 cm and the Reynolds number, $Re = U_0 D/\nu$, was 100. U_0 is the jet exit axial velocity and D is the jet diameter. The forcing cases involved using a velocity function of the form $u = U_0[1 + A\sin(2\pi f t)]$. This function gives a period-averaged velocity of U_0. Based on the amplitude of forcing, there are two regimes for forced jets, the low forcing regime, which has amplitudes less than or equal to 100%, $A < 1$, and the high forcing regime, with amplitudes greater than 100%, $A \geq 1$, and for which flow reversal occurs. One expects the high-amplitude forcing to produce effects quite different than those with low forcing. For the forcing cases the simulations were terminated once time-periodic solutions were obtained.

Table 1 lists the different cases examined in this study. The nondimensional frequency is the Strouhal number, which is defined as $Sr = fD/U_{\max}$, where f is the forcing frequency and $U_{\max}$ is the peak velocity along the centerline at the jet exit.

III. Results

A. Low-Amplitude Forcing

The normalized axial velocity profile for the benchmark steady jet is shown in Fig. 2. Although not shown in Fig. 2, the results are similar to those obtained in a similar computational study by Pai and Hsieh.[17] The axial velocity scales as x^{-1} in the far-field region as suggested by Schlichting.[18] The Schlichting solution, adjusted for the point source of momentum as suggested by Andrade and Tsien,[19] is also shown in Fig. 2.

In Fig. 2 the normalized axial velocity profile for a case identical to that performed by Marzouk et al.[6] is included. The Marzouk et al. case is a low-amplitude forcing problem, $A = 10\%$, with $Sr = 0.273$ and the 25% phase shown. This particular phase has the maximum

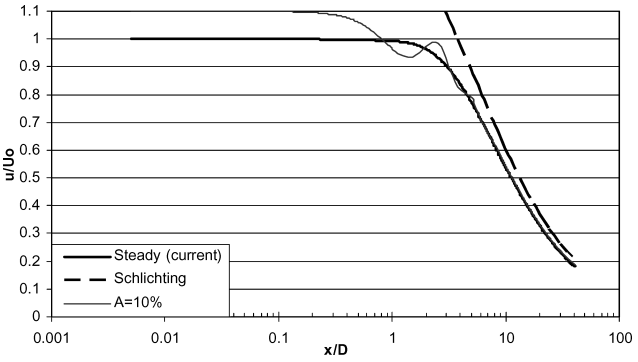

Fig. 2 Validation of centerline velocity, u/U_0, with axial distance, x/D, for steady jets and low-amplitude forcing laminar jets; current steady jet data, $Re = 100$, are compared with analytical solution given by Schlichting,[18] and the low-amplitude forcing case, $A = 10\%$, matches data from Marzouk et al.[6]

jet exit velocity of all of the phases. Consistent with the results by Marzouk et al.,[6] the forcing effects on the axial velocity along the centerline seem to disappear beyond a distance of 8–10 diameters downstream of the orifice, and beyond this downstream distance the profile matches that of the steady-state case. The varying velocity field along the centerline indicates the presence of vortical structures being created at the jet orifice. The decay of the oscillations in the velocity profile indicates that the forcing seems to affect only the jet near-field region and that, farther downstream, the oscillations are attenuated.

B. High-Amplitude Forcing

1. Wall Jets (Without Nozzle)

With higher-amplitude forcing, one expects that the structures generated at the jet entrance plane would get larger and stronger. To examine this, computations with 200 and 300% forcing amplitude over a range of frequencies were performed. Figure 3 shows contour plots of the vorticity field along with the velocity vectors for a steady jet and for five different phases for the forced jet at 200% amplitude forcing and 5 Hz frequency ($Sr = 0.098$). In the steady jet (top left) the vorticity peaks near the orifice (orifice radius of 5 mm) due to the large velocity gradient at the jet exit plane associated with the top-hat profile. As expected, farther downstream, the vorticity magnitudes are reduced as the vorticity diffuses radially outward. For the forced jet, as we move sequentially over the forcing time period, the vorticity field reveals that vortices are being shed off of the orifice edge. The sequence shows the generation of vortices at the orifice edge, followed by their ejection from the near-orifice region and their subsequent convection downstream. This sequence suggests that this case exhibits similarities to an impulsively started jet because the vortices grow in size with downstream distance and convect downstream without interacting with each other. The sequence for a high-frequency forcing case, $f = 50$ Hz and $Sr = 0.98$, at the same amplitude, $A = 200\%$, is shown in Fig. 4. Here too the vortices are ejected from the orifice edge; however, these vortices are not entirely convected downstream. It appears that some parts of the structures are instead pulled back into the orifice. This is in contrast to the low forcing frequency case shown in Fig. 3 where the vortices are convected downstream.

Figure 5a shows the centerline axial velocities normalized by the average exit velocity at five phases for a forcing amplitude $A = 200\%$ and frequency $f = 5$ Hz, corresponding to $Sr = 0.098$. The normalized time-averaged centerline axial velocity profile along the centerline has also been plotted. As expected, the increased forcing amplitude transmits the forcing effects farther downstream as compared to the low-amplitude forcing case (Fig. 2). The normalized time-averaged centerline velocity is larger than unity, over almost 20 diameters ($20D$) downstream, suggesting that the jet volumetric flow rate is larger than that of the steady jet (Fig. 2). Figure 5b shows the same plot for a case with 200% amplitude forcing, but at a higher forcing frequency of $f = 50$ Hz corresponding to $Sr = 1$. This forcing frequency is 10 times the forcing frequency of the

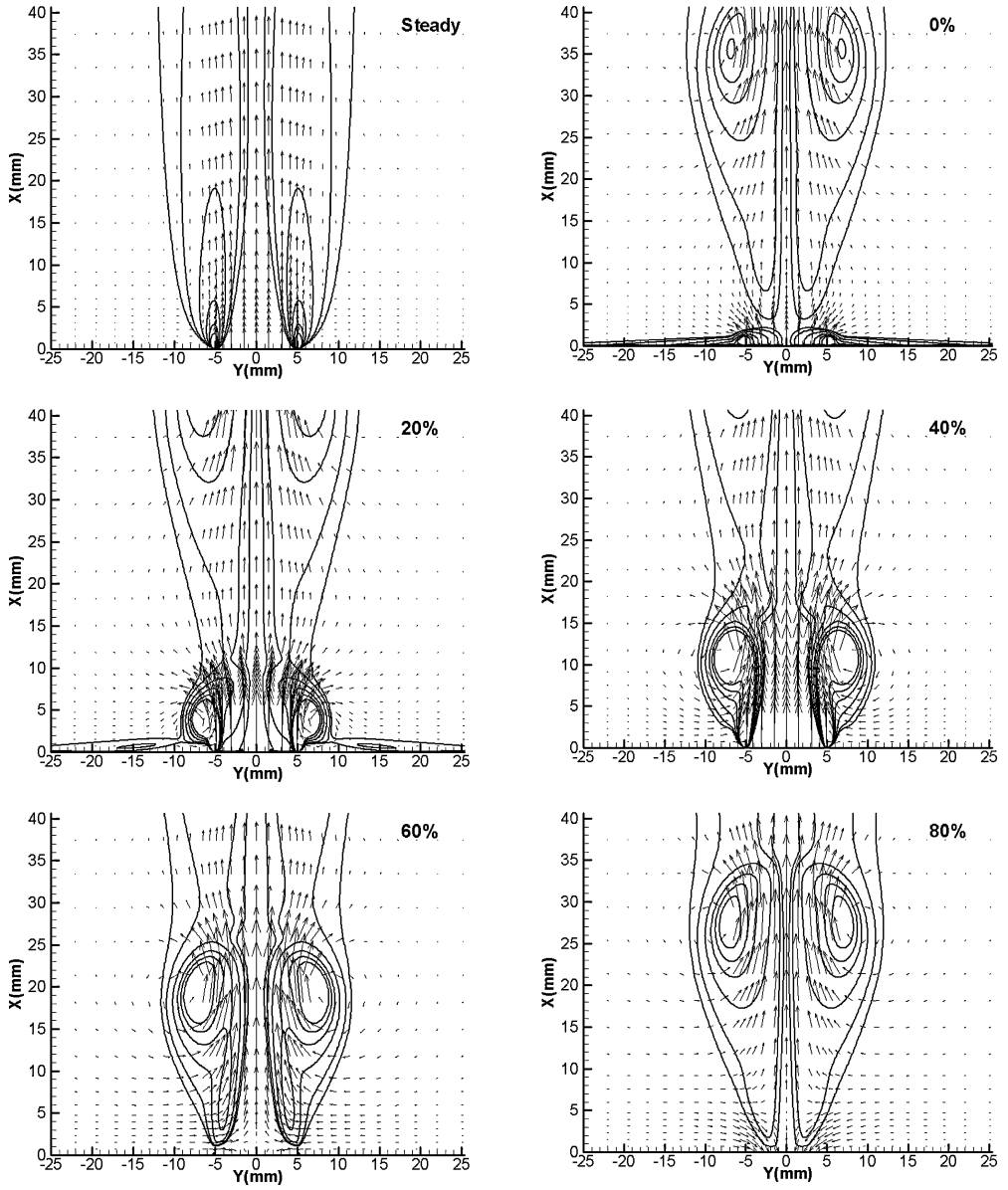

Fig. 3 Vorticity contour plots and instantaneous velocity field for case with forcing amplitude 200% at 5 Hz, $Sr = 0.098$; steady case and five different phases, 0, 20, 40, 60, and 80%, are shown.

case in Fig. 5a, and the increase in frequency affects the region of oscillating flow quite dramatically and shrinks this region closer to the orifice plane. The distance over which the normalized time-averaged centerline axial velocity exceeds unity is slightly smaller (approximately $10D$ downstream) than the low-frequency case, and the peak value of the normalized time-averaged centerline velocity with $Sr = 1$ is higher than that with $Sr = 0.1$. Also, from Figs. 5a and 5b, one can see a region near the orifice plane where the axial velocities are negative. This region is larger for the low-frequency case ($\sim 0.4D$–$0.5D$) than for the high-frequency case ($\sim 0.2D$). Careful viewing of the velocity field time sequences shows that the region in the flowfield where the axial velocity is zero, that is, where the axial velocity changes from negative to positive, is a stagnation point separating a region close to the orifice plane, over which the flow reversal effects dominate the flowfield, and another region away from the orifice over which the flow reversal does not effectively control the flowfield. The velocity vectors in Fig. 3 at the 60 and 80% phase clearly show a stagnation point near the nozzle. This stagnation point is only seen during certain phases (60 and 80% phase) and is created and destroyed over the forcing period. This effect was examined over a range of frequencies (effectively Strouhal number) with a forcing amplitude of 200%. As the forcing frequency increased, the distance over which flow reversal was observed to be reduced. This trend indicates that the forcing frequency appears to be a key factor in the evolution of the velocity field.

On changing the forcing amplitude to 300%, the same trends were observed. An increase in frequency led to a reduction of the region over which the forcing effects were observed. Figure 6 shows the results for the time-averaged centerline axial velocities (normalized by the corresponding peak time averaged centerline velocity), for 300% amplitude forcing and at three different forcing frequencies: 5, 50, and 500 Hz (corresponding to $Sr = 0.074$, 0.74, and 7.4). We normalize by $U_{\max}$ so that we can fit the normalized values in the range from 0 to 1 and compare the different forcing frequency cases. The steady-state profile has also been plotted for comparison. The low-frequency case starts to decay much farther downstream than the steady-state case or the high-frequency forcing cases. Also, the high-frequency forcing cases decay with downstream distance, almost like the steady-state jet. This observation again reinforces the notion that the high frequencies seem to localize the effects of the forcing in the near-orifice region, whereas in the far field the jet behaves similar to a steady jet.

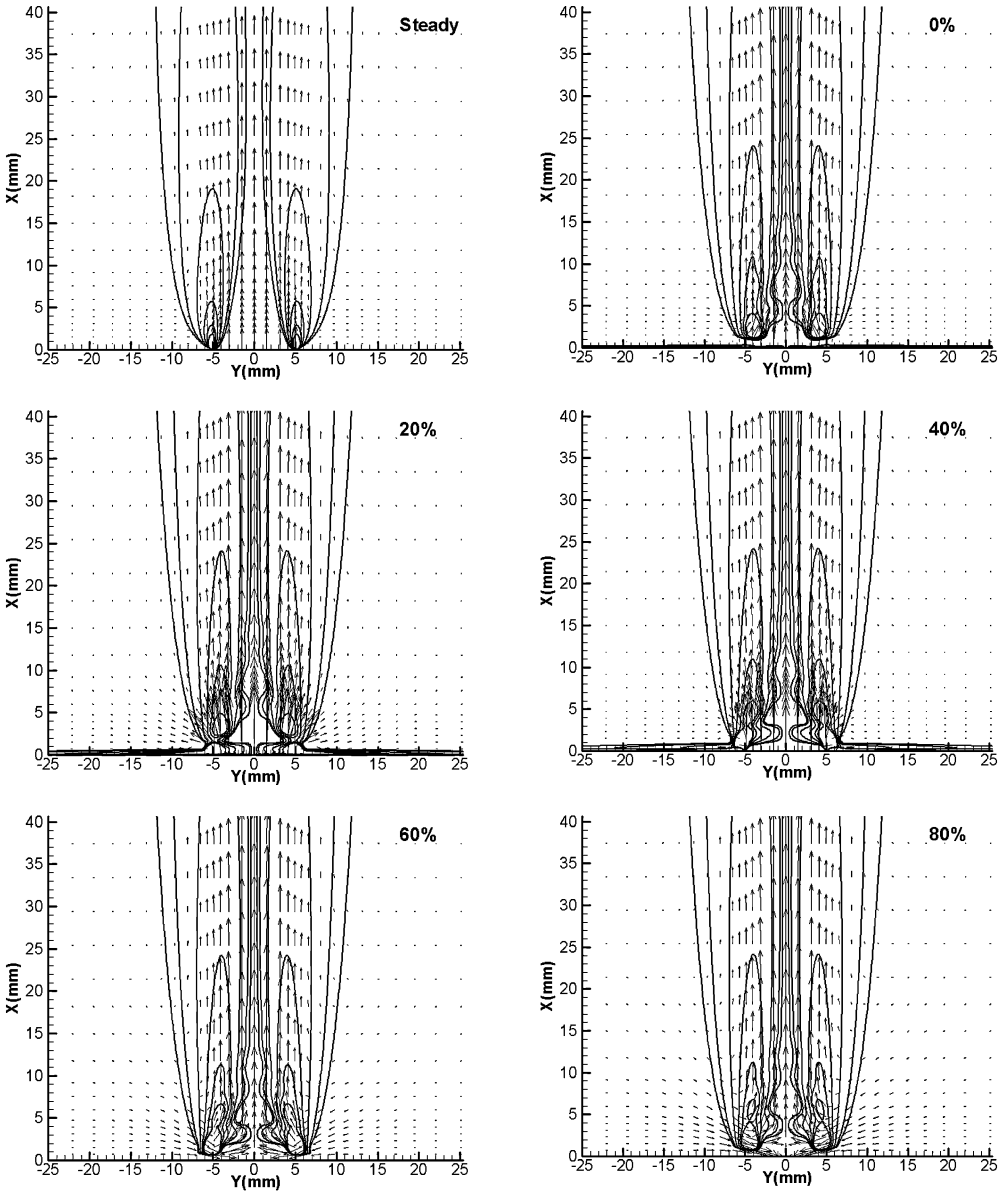

Fig. 4 Vorticity contour plots and instantaneous velocity field for case with forcing amplitude 200% at 50 Hz, $Sr = 0.98$; steady case and five different phases, 0, 20, 40, 60, and 80%, are shown.

Figure 7 shows the time-averaged normalized centerline axial velocity as a function of downstream distance. The profiles have been normalized by their peak values. Figure 7a shows the case of 200 and 300% forcing at a 5-Hz forcing frequency, $Sr = 0.098$ and 0.074, respectively. As expected, the effects of the higher-amplitude forcing, 300%, are felt farther downstream as compared to the low-amplitude forcing at this 5-Hz forcing frequency. For the same forcing amplitudes at a higher frequency, $f = 500$ Hz, no such difference is observed (Fig. 7b), suggesting that differences between 300 and 200% forcing are negligible for high-frequency forcing. Also, at this high frequency, the forced jets decay in a similar manner as the steady jet, even though the normalizing parameter $U_{\max}$ for the two amplitudes and the steady case is different.

In the 200% forcing cases discussed earlier (Figs. 3 and 4), the only difference between the two cases is the forcing frequency. With high-frequency forcing, although the vortices are being generated, they do not seem to have sufficient time to escape the near-field region that exhibits reverse flow. A comparison of the timescales for vortex generation and vortex convection helps us to explain these characteristics. The vortices are generated essentially over the first half of the forcing cycle, giving a vortex generation timescale of $T/2$ [or $1/(2f)$]. The timescale of the convection of the vortices can be thought of as L^*/V^*, where L^* is length of the near-nozzle region that the vortex needs to escape with a characteristic velocity V^*. From Figs. 5a and 5b, along the centerline, the negative velocities are observed over less than $0.5D$. Taking $0.5D$ as the length scale L^* and the peak velocity at the jet exit, $U_{\max}$, as velocity scale V^* gives a vortex convection timescale of $D/2U_{\max}$. $U_{\max}$ appears to be the best choice for the velocity scale because the vortices are shed at the instant at which the velocity peaks. After this peak, the velocity at the jet exit starts to decrease, causing the vortex to separate off of the edge of the orifice. The ratio of the two timescales, vortex generation vs vortex convection, gives $U_{\max}/fD$, which is just the inverse of the Strouhal number.

If the Strouhal number is greater than unity, the vortex generation time is less than the vortex convection time, and the vortices are not shed fast enough to be convected downstream. For a Strouhal number less than one, the vortex generation time is larger than the convection time, and the vortices have enough time to be convected downstream. Gharib et al.[20] and Rosenfeld et al.[21] have used a similar scaling analysis in their study of impulsively started jets and refer to the inverse of the Strouhal number as a "formation time." When the

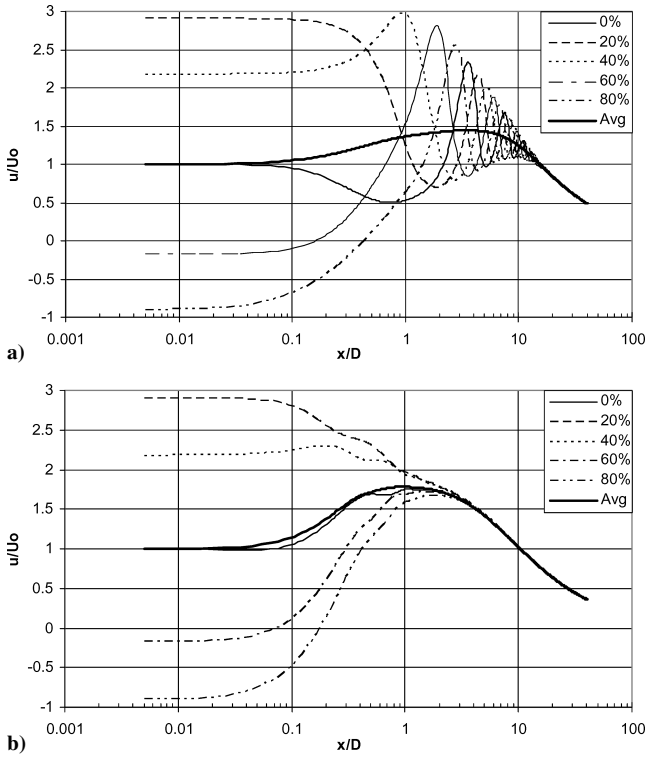

Fig. 5 Centerline velocity vs downstream distance for 200% amplitude forcing at a) 5 Hz, $Sr = 0.1$, for five different phases and b) 50 Hz, $Sr = 1$, for five different phases; time-averaged velocity over cycle also shown, and centerline axial velocity is normalized by mean velocity at jet exit.

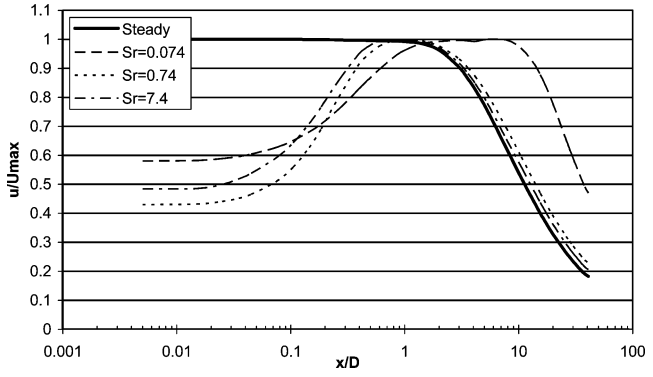

Fig. 6 Time-averaged centerline velocity as function of axial distance with 300% amplitude forcing for Strouhal numbers of 0.074, 0.74, and 7.4; decay of centerline velocity is shown and peak velocity is function of Strouhal number.

terminology by Gharib et al.[20] is used, a short stroke is detrimental to seeing vortex effects downstream because, first, $U_{\max}/2f$ will not create a fully formed vortex. Then, this poorly formed vortex with weak circulation, and, thus, weak induced velocity, is at a distance/stroke $L = U_{\max}/2f$ from the nozzle that is smaller than the critical distance L^* from the nozzle required for a vortex to escape flow reversal. Thus, the two effects together of a weak circulation (incompletely formed vortex) and reverse flow make it less likely that the vortex effects will be felt downstream.

If the Strouhal number is the controlling parameter in periodically forced jets, then at any given forcing frequency f a sufficiently high jet exit velocity $U_{\max}$ should exist such that the Strouhal number is less than unity and the vortices would be convected downstream. These higher velocities can be obtained at the jet exit by using stronger (higher-amplitude) forcing, regardless of the frequencies. To test this hypothesis, a case with the same forcing frequency, $f = 50$ Hz, as that shown in Figs. 4 and 5b, where the vortices are

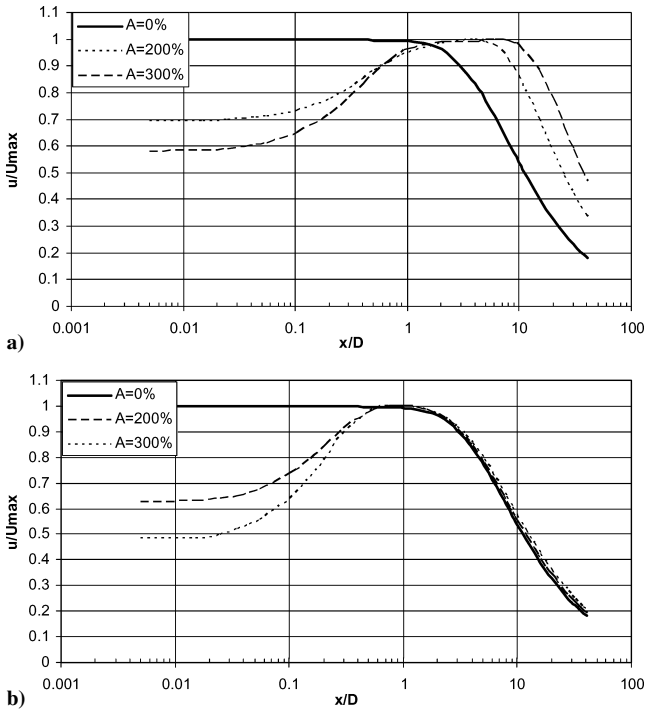

Fig. 7 Time-averaged centerline velocity vs axial distance for a) $f = 5$ Hz and b) $f = 500$ Hz for different amplitudes (200 and 300%).

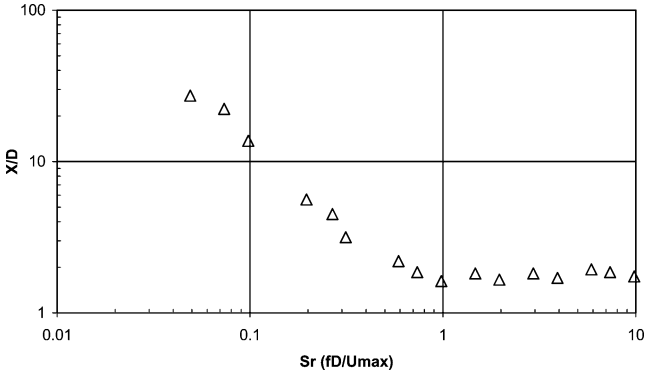

Fig. 8 Axial distance X/D at which velocity oscillations at centerline are no longer seen vs Strouhal number, $fD/U_{\max}$.

not convected downstream, but with a higher forcing amplitude of 1000% instead of 200%, was examined. This case gives a Strouhal number of 0.267 and the vortices were convected downstream of the near-nozzle region, confirming our hypothesis.

Amplitude and frequency modulation appear to control the creation and convection of the vortices, which might prove useful in controlling jet properties. Figure 8 shows the normalized downstream distance, X/D, where the velocity oscillations along the centerline decay to 5% of the time-averaged value for different Strouhal numbers. This downstream distance is an indicator of the distance over which the forcing effects persist for different forcing cases. Figure 8 shows two distinct domains divided by $Sr = 1$. In the region where the Strouhal number is less than one, the downstream decay distance decreases with increasing Strouhal number and scales as $x^{-0.85}$. Beyond $Sr = 1$, the downstream decay distance does not vary with Strouhal number, reflecting the localization of the forcing effects in the near-nozzle region.

2. *Velocity Profile Effects*

Another effect that was considered is the jet exit velocity profile. The 200% amplitude forcing simulations with frequencies of 5, 50, and 500 Hz were repeated with a parabolic (fully developed) profile at the orifice exit. The average flow rate was matched to

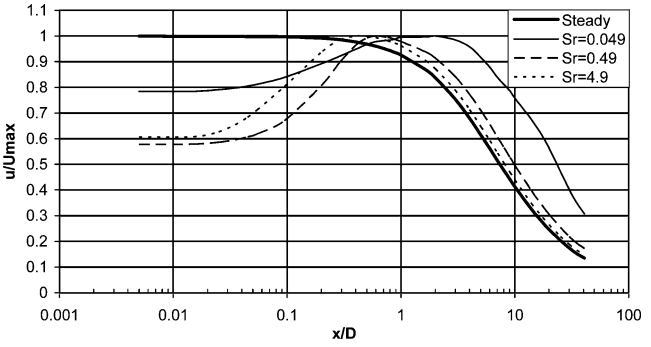

Fig. 9 Time-averaged normalized centerline velocity vs downstream distance for 200% forcing with parabolic velocity profile.

a steady jet with $Re = 100$. The forcing function was of the form $u = U_0(r)[1 + A\sin(2\pi f t)]$, where $U(r)$ is the fully developed Poisseuille velocity profile. Note that, in reality, the forcing frequency would have to be very slow to allow a fully developed profile to exist at the orifice exit. However, we examine this profile as a computational exercise. Figure 9 shows the normalized jet exit velocity, $U/U_{\max}$, along the centerline for three different forcing frequencies (5, 50, and 500 Hz) at 200% amplitude forcing. Here the time-averaged velocity is normalized by the peak value of the time-averaged velocity. As we discussed in the preceding sections, for low-frequency forcing, the oscillations persist farther downstream, whereas with high-frequency forcing (high Strouhal number), the effects are localized. Also, for the high-frequency forcing cases, the normalized velocity decays with axial distance just like the steady case. All of these results are similar to those observed with the top-hat profile, suggesting that the forced jet evolution is relatively insensitive to the exact character of the velocity profiles.

3. *Nozzle Jets*

The next step in the study involved modeling the presence of a nozzle in the computational domain. This domain was shown in Fig. 1b. Kim et al.[22] reported the velocity profiles for an acoustically forced jet. They observed from the velocity profiles at the nozzle exit and within the nozzle that the radial velocity profile was relatively flat and that large gradients existed near the nozzle walls. For our simulations, a top-hat forcing velocity boundary condition was applied at the bottom of the nozzle, that is, at $x = 0$. Figure 10a shows the axial velocity profiles at a location two diameters (2 cm) into the nozzle for a case with 200% amplitude forcing and 50-Hz frequency. An unsteady component of the axial velocity field was also calculated by subtracting off of the corresponding steady-state velocity field. This unsteady axial velocity is shown in Fig. 10b. Consistent with Kim et al.,[22] the profiles show high velocity gradients near the nozzle wall, whereas the profiles are flat over the rest of the cross section. The boundary-layer thickness is approximately 1 mm, which is consistent with a scaling estimate for the Stokes layer at this frequency, $\delta \sim \sqrt{(\nu/f)}$.

Figures 11 and 12 are the vorticity contour and velocity vector plots for 200% amplitude forcing at 5 and 50 Hz, respectively, for the nozzle-resolved calculations. The steady case contour plot is also shown. For the low-forcing-frequency case, the vortices are generated and ejected from the nozzle tips and then convect downstream. During later parts of the cycle, the negative velocities at the nozzle exit can be seen. The axisymmetric geometry of the nozzle results in the fluid being sucked into the nozzle, mainly along the nozzle edge. As a result, during the first half of the cycle where the nozzle exit velocities are positive, the fluid is pushed out over the entire face of the nozzle exit. Over the second half of the cycle, the fluid is sucked into the nozzle primarily along the nozzle walls. Here too, the flowfield generates a stagnation point above the nozzle exit (80% phase case), separating the regions of negative velocity and positive velocity. The high frequency, $f = 50$ Hz, case shows similar results, although the vortices are not convected downstream.

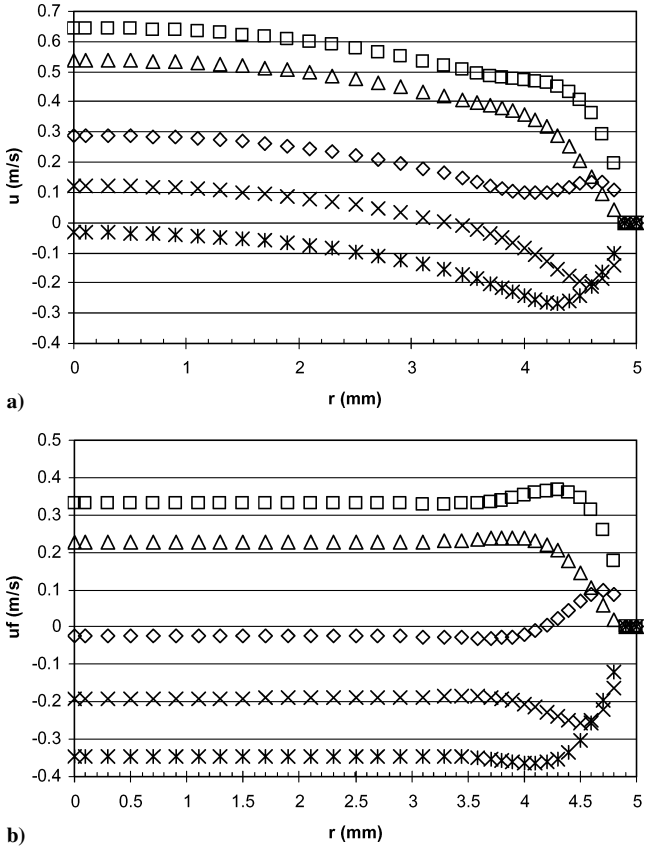

Fig. 10 Plot of a) axial velocity u and b) forced component u_f of axial velocity vs radial distance r at cross section two-dimensional distance within nozzle for 200% amplitude forcing at $f = 5$ Hz, $Sr = 0.098$: ◇, 0%; □, 20%; △, 40%; ×, 60%; and ⁎, 80%.

Figures 13a and 13b show the axial and radial velocity profiles at the first (downstream) grid-point location after the nozzle exit location for forcing at $Sr = 0.098$. The axial velocity profiles at the different phases over the period of forcing show that the effect of the forcing is first felt at the nozzle edge, and then the effects diffuse toward the centerline. In other words, there appears to be a lag along the cross section, and the forcing effects on the velocity in the center lag the effects at the nozzle edge/wall. The steady-state axial velocity profile has also been plotted as a reference. The steady-state axial velocity profile is essentially a fully developed profile based on the entrance length L_e estimate for flow through a pipe, $L_e \sim 0.06\,Re\,D$. The radial velocity profiles explain the lag effects seen in the axial velocity profile. Negative radial velocities indicate fluid motion toward the centerline, whereas positive values indicate fluid motion away from the centerline. During the 60 and 80% phases, the radial velocity is negative, indicating fluid motion toward the centerline. Also, the 0% phase radial velocity is positive as was the 0% phase axial velocity indicating the jet outflow.

Figure 14a shows the normalized centerline axial velocity as a function of the downstream distance for 200% amplitude forcing at 5-Hz frequency, $Sr = 0.098$. The steady-state and the time-averaged profiles have also been plotted for comparison. As has been described earlier, the axial velocity has been normalized by the mean axial velocity of the forcing function at the bottom of the nozzle, $x = 0$. Note that the nozzle length is five diameters, and, hence, the centerline time-averaged axial velocity increases throughout the nozzle. This increase is simply the evolution of the top-hat profile to a Poisseuille profile. The 60% phase velocity profile shows that the axial velocity turns from negative to positive within the nozzle. Immediately downstream of the nozzle exit the time-averaged velocity is larger than the steady-state velocity profile, showing the effect of the redirected ingested mass. Figure 14b is the corresponding plot for high-frequency forcing, $Sr = 0.98$. Just as in the case with the

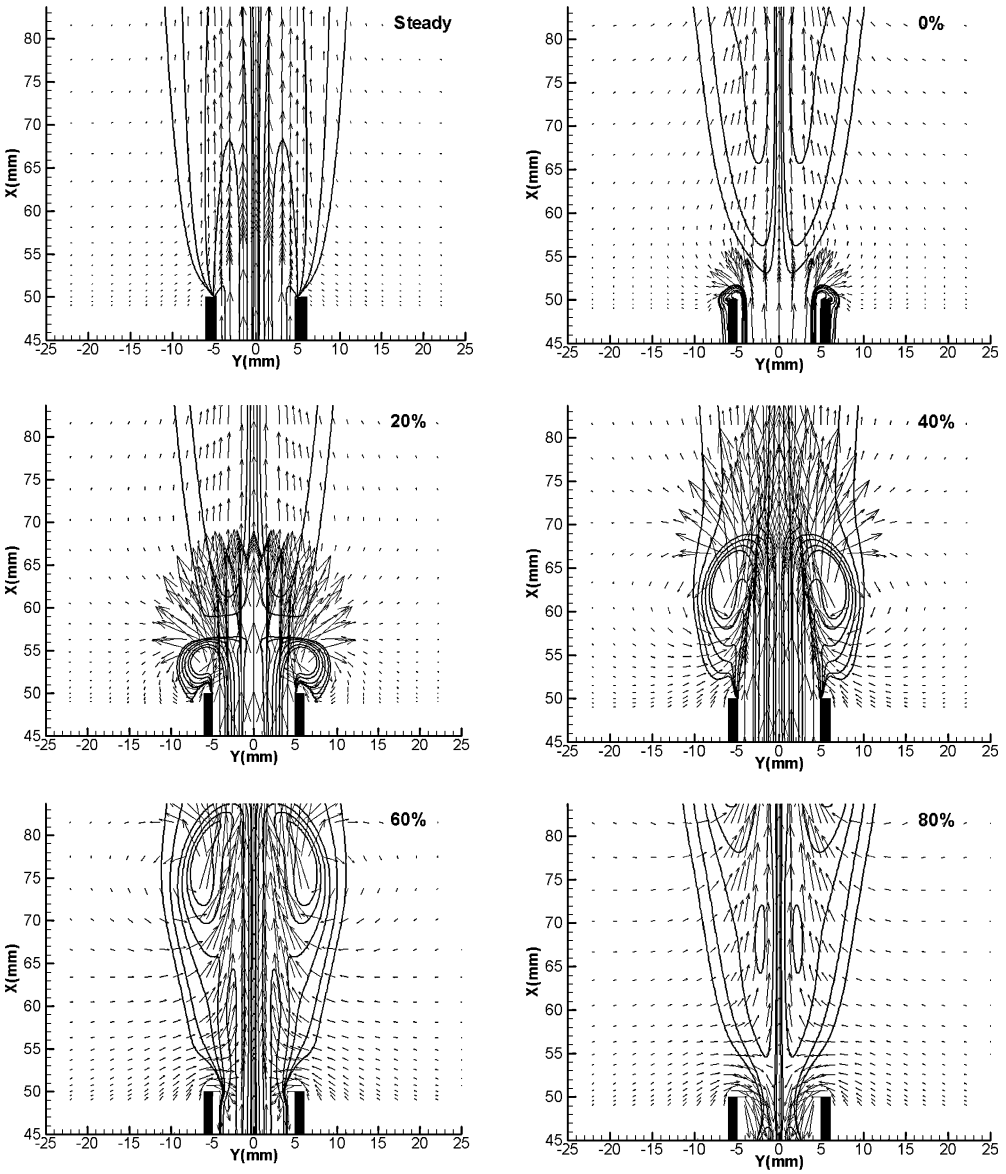

Fig. 11 Vorticity contour plots and instantaneous velocity field for case with forcing amplitude 200% at 5 Hz, $Sr = 0.098$; steady case and five different phases, 0, 20, 40, 60, and 80%, are shown (vorticity values per second).

wall jets, the high-frequency forcing limits the effects of the forcing to the near-nozzle region. Also, the time-averaged velocity profile matches the steady-state profile more closely.

In both (high- and low-frequency-forcing) cases, the peak time-averaged velocities do not differ much from the peak steady-state velocity. This is different from the earlier wall-jet cases, in which the nozzle was not modeled. Note that the peak centerline velocity in the forced and the unforced cases occurs at the nozzle exit. The exit velocity profiles from Fig. 13a show that the centerline axial velocity varies between about 0.65 and −0.15 m/s, whereas the steady-state velocity is about 0.35 m/s. Superficially, this appears to be inconsistent with 200% amplitude forcing. One might believe that 200% forcing of a steady flow with centerline velocity of 0.35 m/s would result in a range of centerline axial velocities from 1.05 to −0.35 m/s. This is not the case. We force a top-hat profile located at the bottom of the nozzle at 200%. The forcing velocity boundary condition at the bottom of the nozzle has a top-hat profile that varies from 0.51 to −0.17 m/s for the case shown in Fig. 13a. Because the profile is flat at the bottom of the nozzle, the centerline axial velocity increases due to the no-slip condition along the nozzle walls. This results in the increase of the positive centerline velocity from 0.51 to 0.65 m/s. However, the peak negative velocity only changes from −0.17 to −0.15 m/s because the strongest negative velocities are seen near the nozzle walls (Fig. 11; 60 and 80% phase).

A comparison of the velocity profiles of the forced jets, with and without the nozzle, is shown in Fig. 15 for a forcing amplitude of 200%. The centerline axial velocity profile of the jets as a function of the downstream distance is plotted. In the case of the jet with the nozzle, the downstream distance has been offset by the nozzle length, so that the downstream distances in both the cases are from the jet exit plane tip. For the low-forcing-frequency case, the velocity profiles with and without the nozzle match one another beyond 10 diameters. This is because the vortices have decayed at these far downstream locations, and the jets now behave as steady jets. However, the high-frequency cases do not match one another over the domain considered. Earlier results (without the nozzle) showed that at high-frequency forcing the jet decays in a similar manner to a steady jet. The steady-state jet exit velocity profile in Fig. 13a shows that the jet, in the case with the nozzle, is close to fully developed. The steady centerline axial velocity decay profiles for the top-hat and parabolic profiles are shown in Fig. 16. These profiles are very similar to those observed in the high-frequency-forcing cases in Fig. 15. Thus, the difference in the high-frequency-axial-velocity profiles can be explained based on the spanwise exit velocity profile. Generally, jets with top-hat and fully developed profiles develop differently because the top-hat profile jet has more initial axial momentum than the fully developed jet with the same mass flux and, hence, decays more slowly than the fully developed jet.

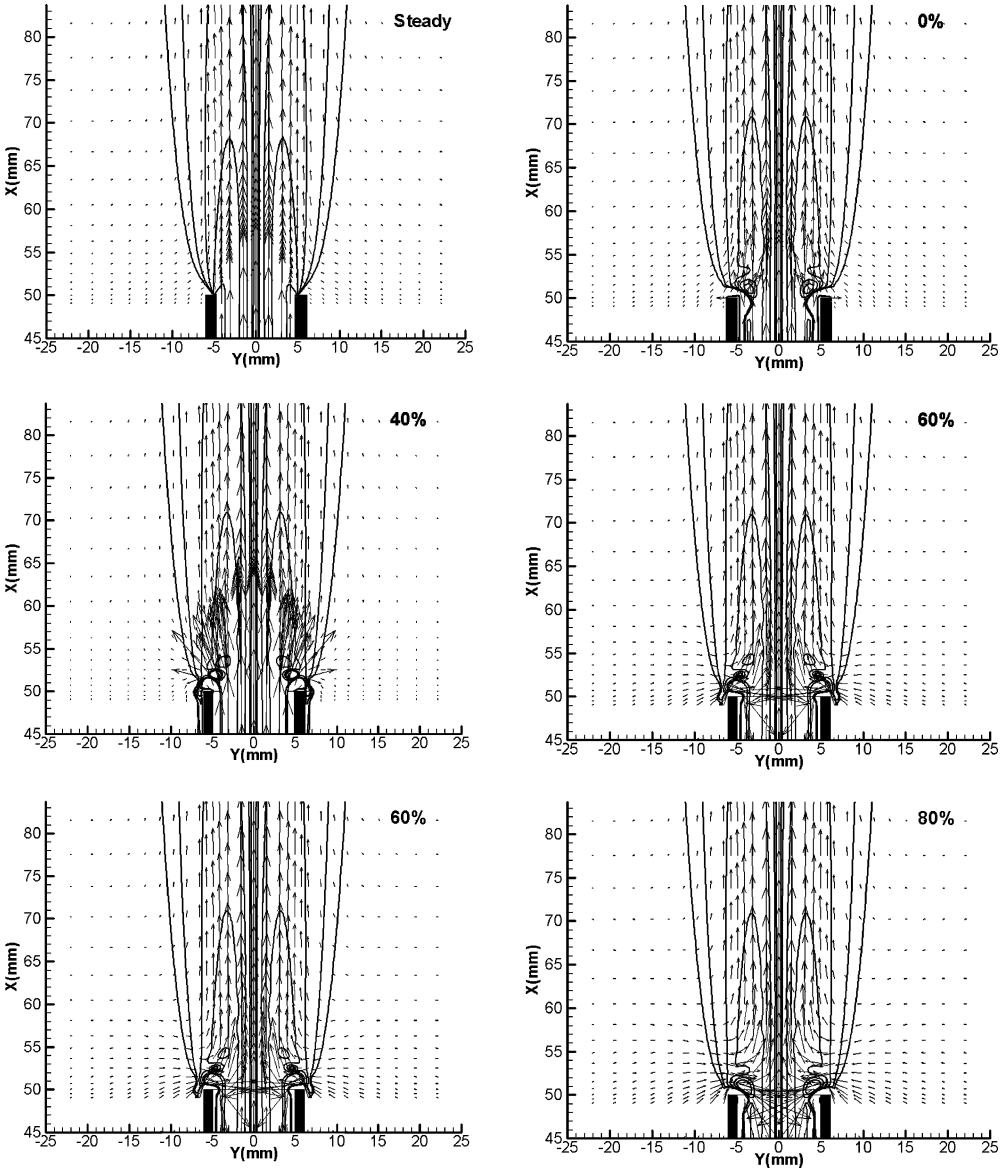

Fig. 12 Vorticity contour plots and instantaneous velocity field for case with forcing amplitude 200% at 50 Hz, $Sr = 0.98$; steady case and five different phases, 0, 20, 40, 60, and 80%, are shown.

C. Jet Spread and Entrainment

Figure 17 shows the half-width of the jet as a function of downstream distance for the steady jet and 200% amplitude forcing jets. The half-width of the jet is the radial distance at which the axial velocity is one-half of the centerline axial velocity. The steady jet half-width compares well with the half-width in Ref. 17. Figure 17 shows that the forced jets do not spread as quickly as the steady jet. The spread rates are calculated at downstream locations where the velocity oscillations have disappeared, and the jet appears to behave like a steady jet. Because there is increased average momentum flux and increased induced volumetric flow rate for the pulsed jet at locations where the pulsed jet is steady, it appears to be a higher-Reynolds-number jet than a steady jet with the same mass flow rate. The lower spread rate appears to be a result of this higher effective Reynolds number of the pulsed jets because it is well known that steady laminar jets spread more slowly as the Reynolds number is increased.

The forced jets are expected to have higher flow rates than steady jets because the forcing action would bring in more fluid from the surroundings. In the current study the entrainment is quantified by the ratio of the volumetric flow rate Q at a downstream cross section to the volumetric flow rate at the nozzle exit Q_e. The volumetric flow rate at a given cross section was calculated as

$$Q = 2\pi \int_0^\infty u(r) r \, \mathrm{d}r \tag{5}$$

Figure 18 shows the entrainment as a function of downstream distance for the 200% forcing cases. The steady-state case has also been plotted for comparison. In the steady case, the slope of the entrainment curve flattens out with downstream distance. This has been observed by Abdel-Hameed and Bellan[23] in simulations of rectangular jets with Reynolds numbers in the 400–600 range. The volumetric flow rate calculations for the forced jets were made at the downstream distances at which the unsteady effects have decayed. For the forced jet cases, the entrainment varies linearly with downstream distance, and at any downstream distance the entrainment in forced jets is higher than that for the steady jet. The forced jets are narrower as compared to the steady jet (Fig. 17) and have higher axial velocities (Figs. 5a and 5b). The forcing action at the orifice edge causes fluid to be sucked into the orifice over part of the forcing period and then pushed out over the remainder of the period. Separation at the orifice plane causes the jet to have higher average axial momentum than the equivalent steady jet with the same mass

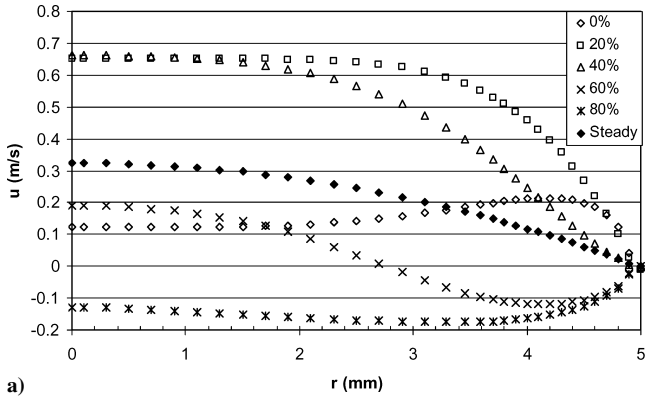

Fig. 13 Velocity profiles a) axial and b) radial at first grid point after nozzle exit for five different phases with 200% amplitude forcing at $f = 5$ Hz, $Sr = 0.098$, and corresponding no-forcing (steady) profile.

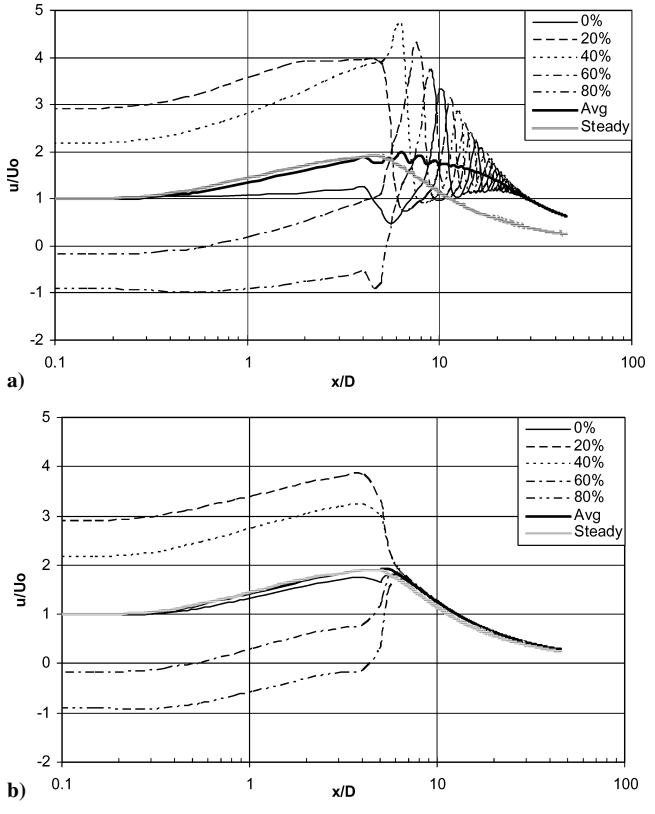

Fig. 14 Centerline axial velocity vs downstream distance for 200% amplitude forcing at a) 5 Hz, $Sr = 0.098$, and b) 50 Hz, $Sr = 0.98$, for five different phases; time-averaged velocity over cycle and steady-state velocity profile are also shown, with centerline axial velocity normalized by mean velocity at bottom of nozzle.

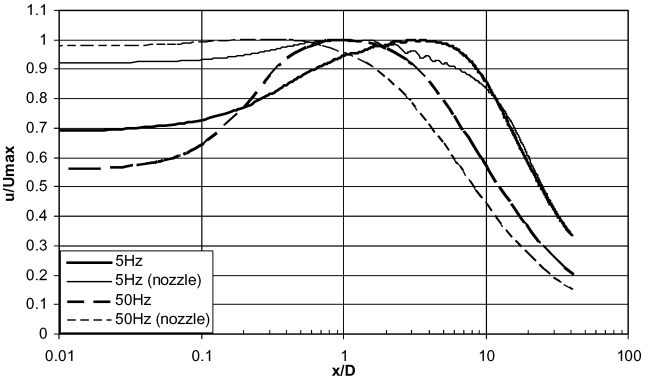

Fig. 15 Comparison of normalized time-averaged centerline axial velocity profiles along centerline, with and without the nozzle for 200% amplitude forcing.

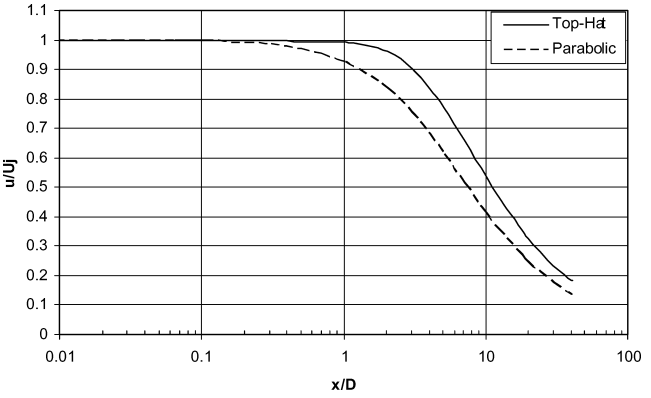

Fig. 16 Centerline axial velocity profiles for steady jets with parabolic profile and top-hat profile.

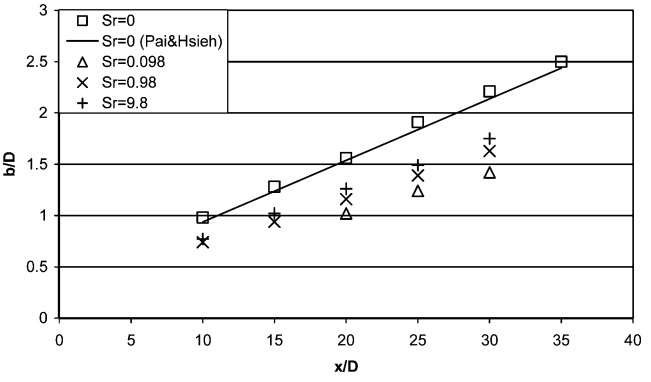

Fig. 17 Half-width of jet as function of downstream distance for 200% amplitude forcing at $Sr = 0.098$, 0.98, and 9.8.

flux. Stated differently, even though the time-averaged flow rate for the forced jets is the same as the flow rate for the steady jet, the directional flow rate (flow rate of the fluid being pushed out) for the forced jets over the time period is higher than the flow rate for the steady jet. This increased flow rate is seen in the higher volumetric flow rates for the forced jets.

Also, the slopes for forced jets are different compared to that of the steady jet. These slopes represent a nondimensional entrainment rate, $D/Q_0(\mathrm{d}Q/\mathrm{d}x)$. For steady laminar jets, the volumetric flow rate at any downstream distance as given by Schlichting[18] is $Q = 8\pi\nu x$. The entrainment rate for the Schlichting correlation is

$$\frac{\mathrm{d}Q}{\mathrm{d}x} = 8\pi\nu$$

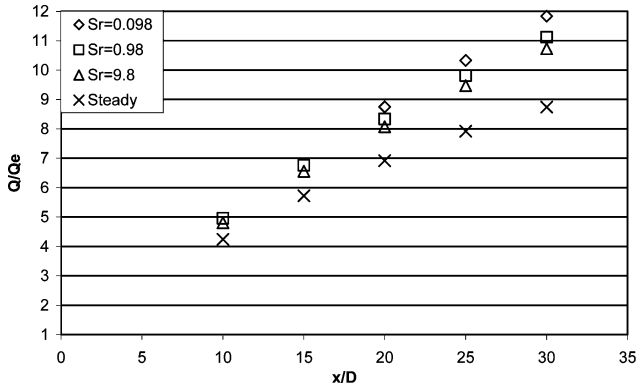

Fig. 18 Entrainment as function of downstream distance for 200% amplitude forcing at $Sr = 0.098$, 0.98, and 9.8.

and nondimensionally,

$$\frac{D}{Q_0}\frac{\mathrm{d}Q}{\mathrm{d}x} = 8\pi\nu\frac{D}{Q_0} = 8\pi\nu\frac{4D}{\pi D^2 U_0} = 32\frac{\nu}{U_0 D} = \frac{32}{Re} \qquad (6)$$

For $Re = 100$, the Schlichting nondimensional entrainment rate is 0.32. In our steady jet calculations, this corresponding value over $x/D < 10$ is 0.324. For the forced cases, the entrainment rates are higher as compared to that of the steady jet. The nondimensional entrainment rate for the steady jet at $x/D = 25$ is 0.18, whereas the corresponding values for the forced jets are 0.3, 0.27, and 0.265 for $Sr = 0.098$, 0.98, and 9.8, respectively.

IV. Conclusions

Simulations of strongly forced axisymmetric jets using a finite volume based CFD code have been performed. The code was benchmarked by simulating a steady jet and low-amplitude forcing jets. The forced jets were simulated using a periodically varying jet axial velocity boundary condition. The peak velocities for the forced jets were three to four times the mean velocity and the forcing frequencies varied from 5 to 500 Hz. The creation and convection of vortices from orifice and nozzle exit planes were studied. The results showed that the Strouhal number was the critical parameter for the downstream evolution of the forced jets. For jets with a Strouhal number less than unity, the vortices were found to convect downstream, whereas with a higher Strouhal number, the forcing effects were localized to the near exit region. Also, for jets forced at high Strouhal number the far-field centerline axial velocity scales with the downstream distance similar to that of a steady jet. The jet exit velocity profile (fully developed or top hat) did not affect these trends, and similar trends were observed for jets issuing from a nozzle (tube five diameters in length). The forced jets were seen to spread slower than steady jets of equivalent mass flow rate. The entrainment calculations showed an increase in volumetric flow rate and entrainment rates for forced jets.

Acknowledgments

This work was supported by the National Science Foundation under Grant CTS-0308589 and NASA under Grant NNC04AA04A.

References

[1]Meldrum, D. R., and Holl, M. R., "Microscale Bioanalytical Systems," *Science*, Vol. 297, Aug. 2002, pp. 1197, 1198.

[2]Lee, Y.-K., Deval, J., Tabeling, P., and Ho, C.-M., "Chaotic Mixing in Electrokinetically and Pressure Driven Micro Flows," *Proceedings of the Micro Electro Mechanical Systems (MEMS)*, Inst. of Electrical and Electronics Engineers, New York, 2001, pp. 483–486.

[3]Crow, S. C., and Champagne, F. H., "Orderly Structure in Jet Turbulence," *Journal of Fluid Mechanics*, Vol. 48, 1971, pp. 547–591.

[4]Hill, W. G., Jr., and Greene, P. R., "Increased Turbulent Mixing Rates Obtained by Self-Excited Acoustic Oscillations," *Journal of Fluids Engineering,* Ser. 1, Vol. 99, No. 3, 1977, pp. 520–525.

[5]Vermuelen, P. J., Rainville, P., and Ramesh, V., "Measurements of the Entrainment Coefficient of Acoustically Pulsed Axisymmetric Free Air Jets," *Journal of Engineering for Gas Turbines and Power*, Vol. 114, April 1992, pp. 409–415.

[6]Marzouk, S., Mhiri, H., Golli, S. E., Palec, G. L., and Bournot, P., "Numerical Study of a Heated Pulsed Axisymmetric Jet in a Laminar Mode," *Numerical Heat Transfer*, Pt. A, Vol. 43, No. 4, 2003, pp. 409–429.

[7]Shaddix, C. R., Harrington, J. E., and Smyth, K. C., "Quantitative Measurements of Enhanced Soot Production in a Flickering Methane/Air Diffusion Flame," *Combustion and Flame*, Vol. 99, No. 3–4, 1994, pp. 723–732.

[8]Papadopoulos, G., Bryant, R. A., and Pitts, W. M., "Flow Characterization of Flickering Methane/Air Diffusion Flames Using Participle Image Velocimetry," *Experiments in Fluids*, Vol. 33, No. 3, 2002, pp. 472–481.

[9]Muramatsu, A., and Era, Y., "Mixing of Carbon Dioxide Gas and Air by a Pulsating Jet with a Reversed Flow," *Proceedings of the 4th ASME/JSME Joint Fluids Engineering Conference*, FEDSM2003-45232, Vol. 2, Pt. D, American Society of Mechanical Engineers, New York, 2003, pp. 2689–2696.

[10]Smith, B. L., and Glezer, A., "The Formation and Evolution of Synthetic Jets," *Physics of Fluids*, Vol. 10, No. 9, 1998, pp. 2281–2297.

[11]Cater, J. E., and Soria, J., "The Evolution of Round Zero-Net-Mass-Flux Jets," *Journal of Fluid Mechanics*, Vol. 472, 2002, pp. 167–200.

[12]Glezer, A., and Amitay, M., "Synthetic Jets," *Annual Review of Fluid Mechanics*, Vol. 34, 2002, pp. 503–529.

[13]Rizzetta, D. P., Visbal, M. R., and Stanek, M. J., "Numerical Investigation of Synthetic Jet Flowfields," *AIAA Journal*, Vol. 37, No. 8, 1999, pp. 919–927.

[14]Lee, C. Y., and Goldstein, D. B., "Two-Dimensional Synthetic Jet Simulation," *AIAA Journal*, Vol. 40, No. 3, 2002, pp. 510–516.

[15]Bera, J. C., Michard, M., Grosjean, N., and Comte-Bellot, G., "Flow Analysis of Two-Dimensional Pulsed Jets by Particle Image Velocimetry," *Experiments in Fluids*, Vol. 31, No. 5, 2001, pp. 519–532.

[16]Katta, V. R., Goss, L. P., and Roquemore, W. M., "Numerical Investigations of Transitional H_2/N_2 Jet Diffusion Flames," *AIAA Journal*, Vol. 32, No. 1, 1994, pp. 84–94.

[17]Pai, S. I., and Hsieh, T., "Numerical Solution of Laminar Jet Mixing with and Without Free Stream," *Applied Scientific Research*, Vol. 27, No. 1, 1972, pp. 39–62.

[18]Schlichting, H., *Boundary-Layer Theory*, 7th ed., McGraw–Hill, New York, 1979, pp. 230–234.

[19]Andrade, E. N., and Tsien, L. C., "The Velocity–Distribution in a Liquid into Liquid Jet," *Proceedings of the Physical Society of London*, Vol. 49, No. 4, 1937, pp. 381–391.

[20]Gharib, M., Rambod, E., and Shariff, K., "A Universal Time Scale for Vortex Ring Formation," *Journal of Fluid Mechanics*, Vol. 360, 1998, pp. 121–140.

[21]Rosenfeld, M., Rambod, E., and Gharib, M., "Circulation and Formation of Laminar Vortex Rings," *Journal of Fluid Mechanics*, Vol. 376, 1998, pp. 297–318.

[22]Kim, T. K., Park, J., and Shin, H. D., "Mixing Mechanism near the Nozzle Exit in a Tone Excited Non-Premixed Jet Flame," *Combustion Science and Technology*, Vol. 89, No. 1–4, 1993, pp. 83–100.

[23]Abdel-Hameed, H., and Bellan, J., "Direct Numerical Simulations of Two-Phase Laminar Jet Flows with Different Cross Section Injection Geometries," *Physics of Fluids*, Vol. 14, No. 10, 2002, pp. 3655–3674.

K. Fujii
Associate Editor